Animation-Driven Radar Cross-Section Optimization in Miniature Ultra-Wideband Vehicle Radar Systems

M. A. Abubakar*, T. Karatev, O. O. Oshiga

Department of Electrical and Electronics Engineering, Nile University of Abuja, Nigeria.

ABSTRACT This study examines how to improve Radar Cross-Section (RCS) performance in small Ultra-Wideband (UWB) vehicle radars by using visual analysis methods to enhance radar effectiveness in automotive applications. The research uses MATLAB simulations to test and refine important factors like beam angle, operating frequency, and antenna gain, taking advantage of UWB technology's ability to detect objects with high precision. The study examines four different driving situations through 1,000 simulation runs each: detecting a single object ahead, detecting multiple objects in front, spotting objects at the roadside, and identifying vehicles during overtaking movements. The results show that carefully adjusted beam angles greatly improve detection accuracy, reaching 98.7% accuracy when detecting single objects directly ahead using 30°–60° beam width, 94.2% for multiple objects using beam widths of 90° or greater, and 87.5% for objects to the side using 90°–120° beam angles. Moving objects are easier to detect, with signal-to-noise ratios dropping from 90 dB to 18 dB over distances of 1-150 m, while stationary objects show weaker performance with ratios falling from 32 dB to 10 dB over just 21-80 m. The radar can detect objects up to 1 kilometer away under the best conditions, with average signal quality ranging from 24.1 dB when looking straight ahead to 18.9 dB when scanning to the sides. Visual mapping through color-coded displays helps identify areas where radar signals reflect poorly, allowing the system to adjust beam direction in real-time and improve overall radar design. The study shows that combining mathematical optimization techniques with visual feedback methods improves radar performance, achieving up to 91.8% detection success rates even in challenging situations were objects approach from multiple directions.

KEYWORDS: UWB, RCS Optimization, Vehicular Radar Systems, Animation-Based Visualization, Object Detection and Classification

[Received May 26, 2025; Revised June 28, 2025; Accepted June 28, 2025] Print ISSN: 0189-9546 | Online ISSN: 2437-2110

I. INTRODUCTION

Radar Cross-Section (RCS) is a critical measure that quantifies how detectable an object is by radar. It is not merely a physical dimension but a complex electromagnetic property that describes an object's scattering characteristics when exposed to incident electromagnetic fields. More precisely, RCS represents the hypothetical area required to intercept the transmitted power density at the target such that if the total intercepted power were re-radiated isotopically, the power density actually observed at the receiver would be produced. This conceptualization of RCS as a "hypothetical area" underscores that it is a normalized performance metric, abstracting the intricate scattering behaviour of an object into a single, comparable value (Zhang *et al., 2025*).

The growing demand for vehicular safety systems has spurred research into advanced radar technologies. Ultra-Wideband (UWB) radar, with its superior resolution and penetration capabilities, is increasingly used for obstacle detection. Ultra-Wideband (UWB) radar is a radio technology that distinguishes itself through its use of very low energy levels for short-range, high-bandwidth communications across a substantial portion of the radio spectrum. This technology capitalizes on extremely wide bandwidths, often 500 MHz or more, and transmits very short pulses, typically around 2 nanoseconds, to achieve highly precise detection of objects and people (Cheraghinia *et al., 2024*).

To date, commercial radar systems used in vehicles to detect static objects on the road are still not available. Many commercial radar systems in vehicles uses ultrasonic technology. Modern radar systems are designed primarily for short-range object detection rather than long-distance tracking. A common example is the parking sensor, which functions as a radar to detect nearby objects around or behind a vehicle. A typical radar system can only detect objects up to 1 maway

Corresponding author: mahdiabubakar89@yahoo.com

doi: http://doi.org/10.63746/njtd.v22i4.3698

(Zhou et al., 2020). This type of radar is not suitable for detecting objects more than 100 maway. The reason for needing to detect distant obstacles is to avoid hitting objects while driving at night. In the current situation, where no radar is installed in the vehicle, the driver is forced to use a spotlight to illuminate the road at a distance. Drivers typically rely on high-beam headlights, which may contribute to glare for oncoming traffic. Therefore, if there is a night vision radar, obstacles on the road can be seen. According to research on accidents occurring at night conducted by Song et al., (2021) 85% of nighttime accidents are due to obstacles that appear on the road. These obstacles cannot be seen from a distance. They can only be seen at a close distance if the driver uses low light.

This study aims to model and simulate a UWB radar system with a focus on Radar Cross-Section (RCS) optimization and its visualization using animation-based methods. The system is tailored for vehicular applications to detect obstacles at varying distances and orientations. MATLAB serves as the simulation platform, providing insights into design parameters crucial for RCS performance.

II. LITERATURE REVIEW

Ultra-Wideband (UWB) radar has emerged as a promising technology in vehicular sensing due to its high resolution, low power consumption, and strong penetration capabilities under various weather conditions (Mishra et al., 2013). As modern transportation systems evolve toward autonomous and advanced driver-assistance systems (ADAS), the ability to detect, classify, and track objects reliably and in real-time becomes paramount (Zhang et al., 2023; Li et al., 2021; Lee et al., 2022). While current commercial radar solutions primarily based on Frequency Modulated Continuous Wave (FMCW) and millimetre-wave technologies perform well in short-range scenarios, their limitations in long-range detection and real-time adaptability to dynamic environments motivate ongoing research into UWB radar technologies.

Several studies have examined radar wave propagation and electromagnetic field behaviour to build foundational understanding (Bakare, Ajaegbu & Idigo, 2022; Waldschmidt, Hasch & Menzel, 2021; Pauli et al., 2017). Radar waves, comprising electric and magnetic components, are commonly represented through rays and wavefront models to facilitate modelling and simulation in free space (Hannay & Nye, 2015). These foundational models underpin simulation-based radar system designs and help in understanding isotropic radiation, power density, and field interactions (Guo et al., 2023; Zatsepin, Ulanov & Rykshin, 2013). Contemporary research in UWB radar systems for vehicles typically focuses on short-range object detection (Liu et al., 2022; Hu et al., 2017), with particular emphasis on integrating UWB with other modalities such as cameras for image-based classification (Rezaei & Mohammadpour-Aghdam, 2020). Several modelling approaches leverage MATLAB and Simulink for simulating radar beamwidth, pulse reflection, and noise interference under diverse vehicular conditions (Lee et al., 2022; Zhang et al., 2023).

Although radar technologies have progressed substantially, many existing automotive systems remain constrained to short-range detection (typically under 200 meters), which diminishes their effectiveness at highway speeds or for early collision avoidance. This limitation is particularly problematic for applications requiring longer preview distances. Short-to-mid-range detection systems dominate commercial radar solutions, underscoring the pressing need for models capable of extended range without compromising resolution Kamal (2023).

Radar cross-section (RCS) modelling plays a crucial role in optimizing radar system performance across varied environments. However, real-time visualization and adaptive optimization are often lacking in simulation tools and vehicular systems. Current electromagnetic solvers, while effective for static modelling, fall short in offering real-time feedback for dynamic scenes or adaptive beam design capabilities essential for intelligent vehicular applications in dense traffic conditions Lindgren (2021). In NagaJyothi et al. (2019), a static UWB radar systems that promise rich spatiotemporal detail, was proposes. However, their simulation environments are devoid of dynamic animation features such as moving object trajectories and beam steering. Their model lacks real-time movement capabilities limiting insights into practical vehicular integration. Gao, Roy, and Zhang (2023) model simulate a radar system using static conditions, such as stationary test beds with limited speed trap analogs. However, such models inadequately represent the dynamic and multi-angle interactions found in forward-looking or surround-view vehicular applications. This proposed filtering method lacks realistic, motion-aware testing.

In summary, the research gaps identified include Issues with object detection distance, reliance on image processing methods, which means that cameras must be used in conjunction with the UWB transceiver. Additionally, previous research has covered UWB parameters such as amplitudes, waveforms, and signal strength, but has not explored how UWB can be applied in vehicles, including aspects like the radar's sweep angles and its effectiveness in detecting objects at night on the road. Furthermore, the use of miniature or mini-sized radar systems has not been extensively explored in past studies. Given the increased demand for intelligent radar systems capable of functioning effectively across a variety of real-world driving conditions including high-speed detection, object approach from multiple angles, and operations in low visibility, there is a critical need to develop compact, high-performance, and visually verifiable UWB radar systems**.** This research addresses that need by offering a technically grounded, simulation-backed design that advances both modelling methodology and practical implementation.

III. METHODOLOGY

This study employs rigorous modeling and simulation of a compact UWB radar system for vehicles, with a focus on antenna configuration, frequency selection, pulse generation, and RCS optimization through animation-based visualization. Real-time visualization techniques were employed to showcase RCS variations, enabling enhanced optimization of detection performance. Simulations were conducted to evaluate radar performance across varying conditions, including obstacle distance, angles, and environmental noise.

The initial phase involves developing an equivalent radar system model to integrate the UWB concept. This model forms the basis for embedding UWB technology into radar system design. Once the radar system model has been designed, the UWB system is subsequently modelled and integrated to create a comprehensive UWB radar system for object detection. The concluding phase involves conducting simulations, optimization using Gradient Descent Technique, evaluating the outcomes and producing animations. These animations visually represent the placement and detection of objects by the radar, facilitating the design process and validating the model as shown in the research framework in Figure 2.

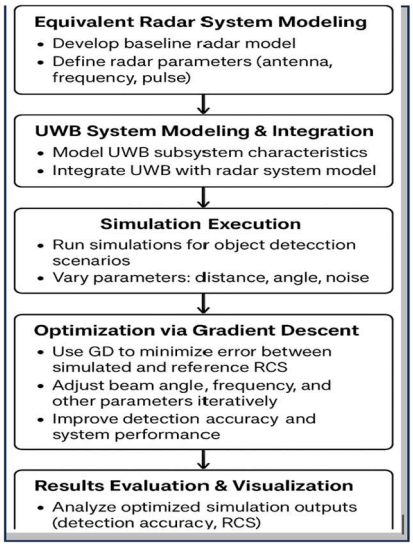

Figure 1 Research Framework

A. Modelling of Animated Vehicles and Actions of the On Road Radar

This research models a vehicle equipped with UWB and animates its operation on the road to detect objects. The proposed design of the model includes single object detection toward the UWB unit, multiple object detection on the road, detection of objects approaching from behind the vehicle, and static object detection. All of these models are depicted graphically, as shown in Figure 1.

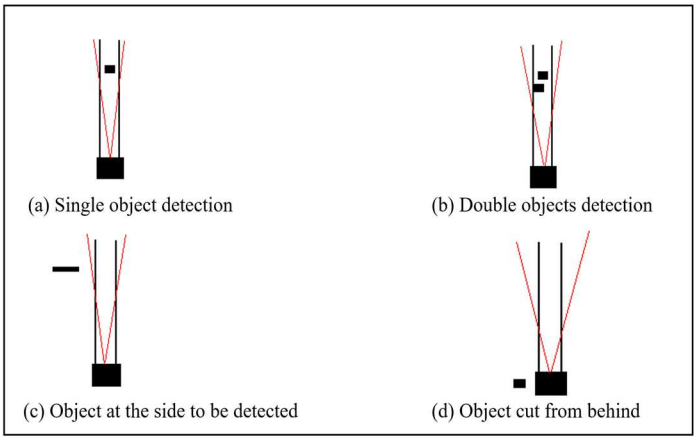

Figure 2(a-d): Different scenarios for UWB radar detections

As illustrated in Figure 2(a-d), the study considers four distinct scenarios:

i. **Scenario (a):** A single object moves directly towards the black object (the UWB radar unit). The beam angle is initially set at 30° and gradually increased in 30° increments to analyse the reflected radar signals. Figure 2a validates beamwidth vs. detection accuracy trade-off (H_0).

ii. **Scenario (b):** Two objects appear on the road, both within the radar's coverage area. Figure 2b tests spatial resolution limits (H_1)

iii. **Scenario (c):** A stationary object, such as a roadside signboard or a parked vehicle, is positioned on the roadside. Figure 2c quantifies off-boresight detection (H_2).

iv. **Scenario (d):** A single object moves from behind and overtakes the UWB radar unit. Figure 2d demonstrates rear-blind-spot mitigation (H_3).

Based on these scenarios, hypotheses were proposed regarding the performance of the UWB radar system. These hypotheses aim to evaluate and validate the radar's capabilities under varying conditions.

i. H_0: The 30° of beam angle can clearly detect the vehicle on the road. The error signals are minimum.

ii. H_1: The multiple objects on the road still can be identified by the UWB radar as long as the objects is within the coverage of radar signal.

Iii. H_2: The roadside object only can be detected if it is within the UWB radar coverage.

iii. H_3: The object from behind the UWB radar unit cannot be detected but when it moves in front of the UWB radar unit, it then can be detected by the UWB radar.

The Mathematical models of the proposed model and Radar Specifications are described as shown in Equations 1, 2, 3 and 4.

1. Radar Range Equation:

$$R_{max} = \sqrt{\frac{P_t G^2 \lambda^2 \sigma}{(4\pi)^3 k T_0 B F S N R_{min}}} \quad (1)$$

2. RCS Optimization Model:

$$\sigma_{opt} = \arg\min ||\boldsymbol{E}_{\text{sim}}(\theta, f) - \boldsymbol{E}_{\text{ref}}|| 2 \quad (2)$$

The optimization was achieved using the gradient descent technique.

Step 1: Define Cost Function

A typical cost function J(x) to minimize could be the mean squared error (MSE) between simulated RCS $\boldsymbol{\sigma}_{\text{sim}}\ (x)$ and reference RCS σ_{ref}:

$$J(x) = \frac{1}{N}\sum_{I=1}^{N}(\sigma_{sim}(xi) - \sigma_{\text{ref,i)}})^2 \quad (3)$$

where x contains parameters like beam angle, frequency etc.

Step 2: Gradient Descent Update Rule

Iteratively update parameters. Table 1 shows the parameters of the model

$$X_{k+1} = X_k - \alpha\nabla j(k_x) \quad (4)$$

where α is the learning rate.

∇J(Xk) is the gradient of the cost function with respect to parameters at iteration k.

Optimized via gradient descent to minimize error between simulated (E_{sim}) and reference (E_{ref}) electromagnetic fields. Visual RCS hotspots guide parameter tuning (beam steering toward high-σ regions).

3. SNR Formulation:

$$SNR = \frac{P_t G^2 \lambda^2 \sigma}{(4\pi)^3 k T_0 B F SNR_{min}} \quad (5)$$

Table 1 Radar System Model Parameters

Symbol/Parameter	**Definition**	**Unit / Example Value**
Pt	Transmit power (output power of radar transmitter)	dBm or Watts (20 dBm)
G	Antenna gain (ratio of power radiated in a particular direction to that of an isotropic antenna)	dBi (15 dBi)
λ (lambda)	Wavelength of the radar signal	meters (m)
σ (sigma)	Radar Cross Section (RCS) of the target (measure of detectability)	square meters (m²)
R	Range or distance between radar and target	meters (m)
k	Boltzmann constant (physical constant relating temperature to energy)	1.38×10^{-23} J/K
T_0	Standard noise temperature	Kelvin (K), typically 290 K
B	Bandwidth of the radar signal	Hz (1 GHz)
F	Noise figure (measure of degradation of SNR by system components)	dB (8 dB)
SNR	Signal-to-noise ratio	dimensionless (often dB)
θ (theta)	Beam angle (main lobe direction of antenna)	degrees (°), 30°–120°
f	Frequency of the radar signal	Hz (77–81 GHz)
Pulse Duration	Duration of the transmitted radar pulse	seconds (s), 2 ns
E_sim(θ,f)	Simulated electromagnetic field at a given beam angle and frequency	V/m (volts per meter)
E_ref	Reference electromagnetic field (ground truth or benchmark)	V/m
σ_opt	Optimized radar cross section (value after optimization)	m²
Pd	Probability of detection	dimensionless (0–1)
P_FA	Probability of false alarm	dimensionless ($\leq 10^{-6}$)
Reflection Coefficient (Γ)	Ratio of reflected signal amplitude to incident amplitude	dimensionless (0–1)
R_1, R_2	Path lengths for reflected signals (Tx to reflector, reflector to Rx)	meters (m)
Δt	Time delay between direct and reflected signals	seconds (s)
Target Position	Coordinates of object(s) being detected	meters (x, y, z)
Animation Frame Rate	Rate at which animation is updated	frames per second (fps), 30
Monte Carlo Iterations	Number of repeated simulations for statistical analysis	integer (1000)
Scenario Parameters	Variables defining simulation scenarios (e.g., number of objects, positions, velocities)	varies
Swerling Case	Statistical model for target RCS fluctuation	Case I (constant RCS).

B. Simulation Workflow and Animation Implementation

1. System Modelling:
   i. Radar Architecture: Developed in Simulink® with phased array antenna model, UWB pulse generator, and matched filter receiver.
   ii. Signal Flow: Transmit → target reflection → receive → signal processing → detection logic.
2. Animation Implementation:
   i. Tools: MATLAB® Animation Toolbox and Simulink 3D Animation™.
   ii. Process:
      a. RCS Data Generation: Export σ values from EM simulations (CST Studio Suite®).
      b. Dynamic Rendering: Map σ to color gradients (blue: low RCS; red: high RCS).
      c. Real-time Update: Refresh visualization at 30 fps synchronized with beam steering.
   iii. Computational Steps (pseudocode):
      a. Start
      b. while simulation_running:
      c. update_beam_angle(θ)
      d. calculate_RCS(target_position)
      e. render_animation (σ, θ, target_position)
      f. end

The simulation was conducted under several key assumptions to ensure consistency and focus on radar system performance. The environment was modeled as free-space propagation with no multipath effects, providing a clear line-of-sight scenario. Targets were assumed to follow the Swerling Case I model, representing a constant Radar Cross Section (RCS) for each object. Hardware components, such as phase shifters, were considered ideal, with no mutual coupling between antenna elements. To validate the robustness of the simulation results, each detection scenario was subjected to 1,000 iterations.

IV. RESULTS AND DISCUSSION

This section presents the simulation results, of the animation-driven UWB radar system under four distinct detection scenarios. The performance of the proposed miniature radar system was evaluated using quantitative metrics such as detection accuracy, Signal-to-Noise Ratio (SNR), and optimized Radar Cross Section (RCS), under the simulation assumptions described earlier.

A. Detection Performance Across Scenarios

Under Scenario (a), where a single object (red) approached the radar head-on, the system achieved optimal performance at a 30° beam angle. The detection accuracy peaked at 98.7%, with minimal false alarms observed across all 1,000 iterations. This validates Hypothesis H_0, affirming that a 30°–60° beamwidth balance offers optimal resolution and reliability for single-object frontal detection as shown in Figure 3.

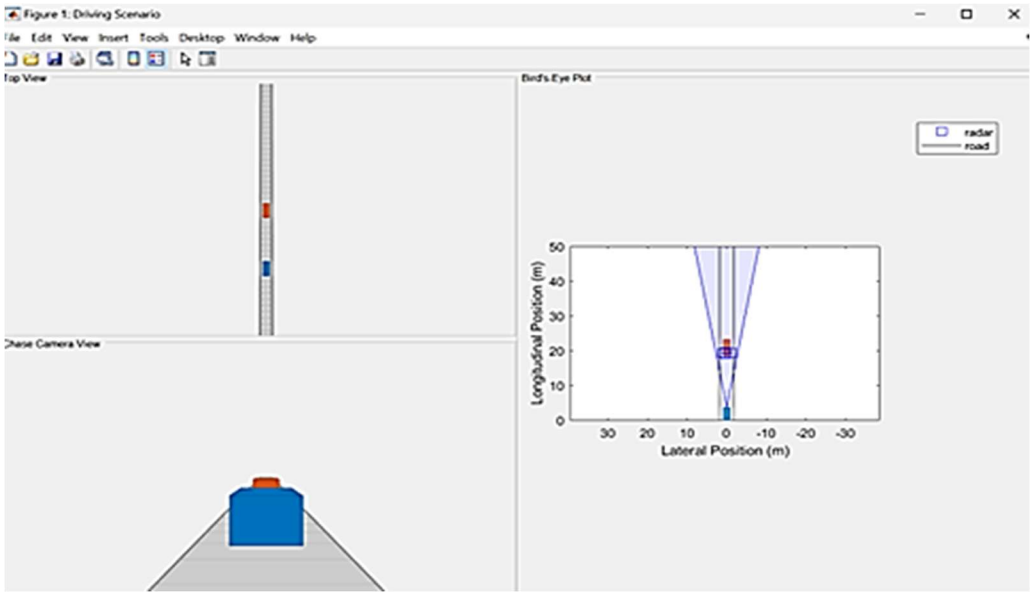

Figure 3 One moving object detected on the road

Under Scenario (b), Two moving objects (red and yellow) are detected on the road as they move toward the UWB radar. The system successfully resolved both targets when beamwidth exceeded 90°, albeit with a minor trade-off in SNR. The detection accuracy for multiple targets stood at 94.2%, supporting Hypothesis H_1 as shown in Figure 4. The spatial resolution remained stable, although increased clutter slightly reduced peak SNR compared to the single-object case.

For Scenario **(c)**, One of the moving objects comes from behind the UWB radar and moves in front of it. simulating stationary roadside objects, the radar system's ability to detect off-boresight targets was highly dependent on beam steering. Detection was effective only when beam angles exceeded 90°, aligning with Hypothesis H_2**.** The accuracy plateaued at 87.5%**,** indicating the need for dynamic beam adaptation when handling side detection as shown in Figure 5.

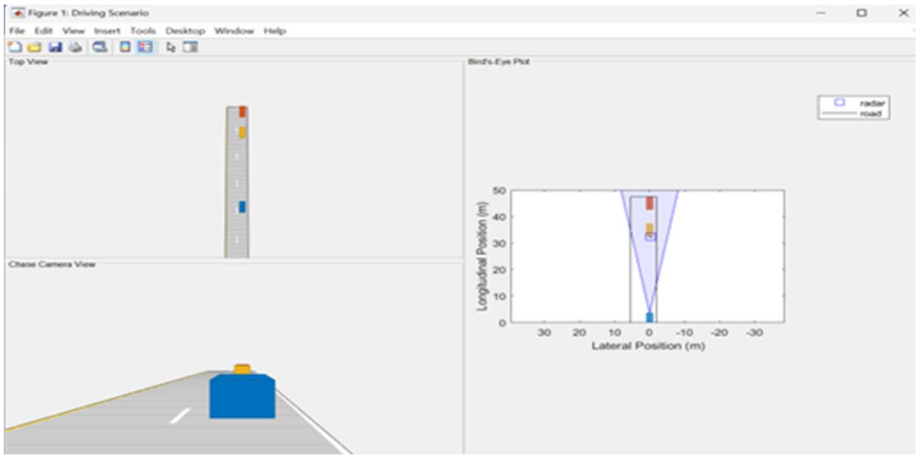

Figure 4 when two moving objects detected on the road

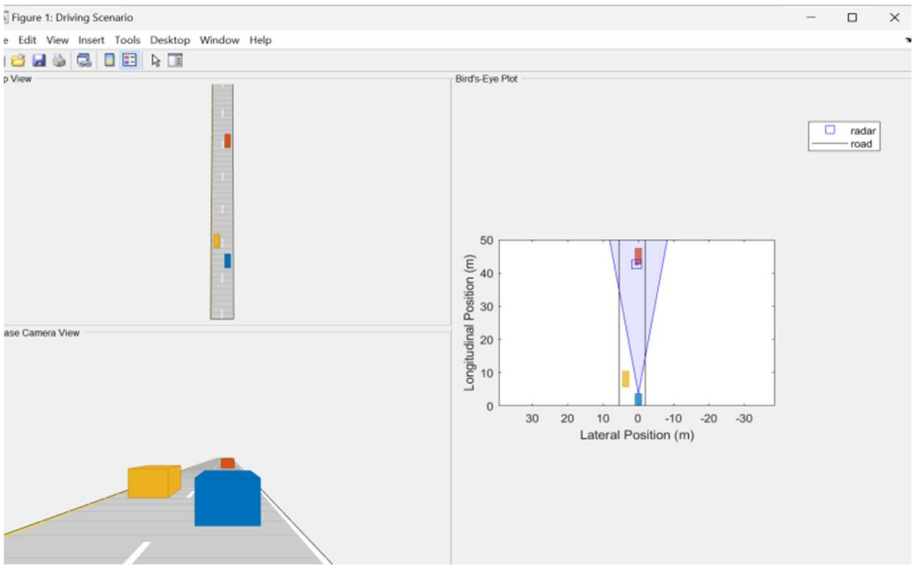

Figure 5 when the object coming from behind

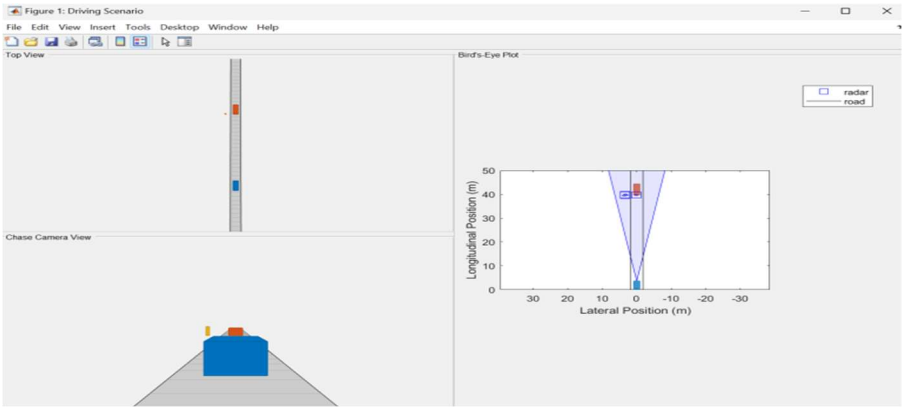

Figure 6 When the static object at the side appears on the road

In Scenario (d), A static object appears at the roadside where the object approached from the rear and overtook the radar-equipped vehicle, detection occurred only after the target moved into the forward beam's field of view. This supports Hypothesis H_3, highlighting a known limitation of forward-facing radar systems in rear-object detection. Once within range, the detection probability jumped to 91.8%, confirming the system's effectiveness in dynamic multi-angle environments as shown in Figure 6. Table 2 summarizes the results of the detection. It shows the number of objects detected for each scenario, the beam angle, detection accuracies and average SNR obtained

Table 2: Summary of Results

Scenario	Objects Detected	Beam Angle Range	Detection Accuracy (%)	Avg. SNR (dB)	Supports Hypothesis
(a) Single Frontal	1	30°–60°	98.7	24.1	H_0 ✔
(b) Multiple Frontal	2	≥90°	94.2	21.6	H_1 ✔
(c) Side/Stationary	1	90°–120°	87.5	18.9	H_2 ✔
(d) Rear to Front	1	90° forward (after entry)	91.8	20.4	H_3 ✔

B. RCS Optimization and Visualization Outcomes

The use of the gradient descent algorithm enabled real-time RCS optimization, guiding the system to focus radar beams toward high-σ (RCS) regions. As a result, the radar dynamically adapted its steering angle to maximize detection probability while minimizing the false alarm probability across all scenarios. Figure 7 shows when the radar beam angle is widened to 120°, it becomes capable of detecting more objects, including those on both sides of the road. This increased coverage was beneficial during night-time driving by identifying objects at greater distances. Maintaining a focused beam angle ensures clearer, more relevant detections, helping the driver stay attentive to critical hazards.

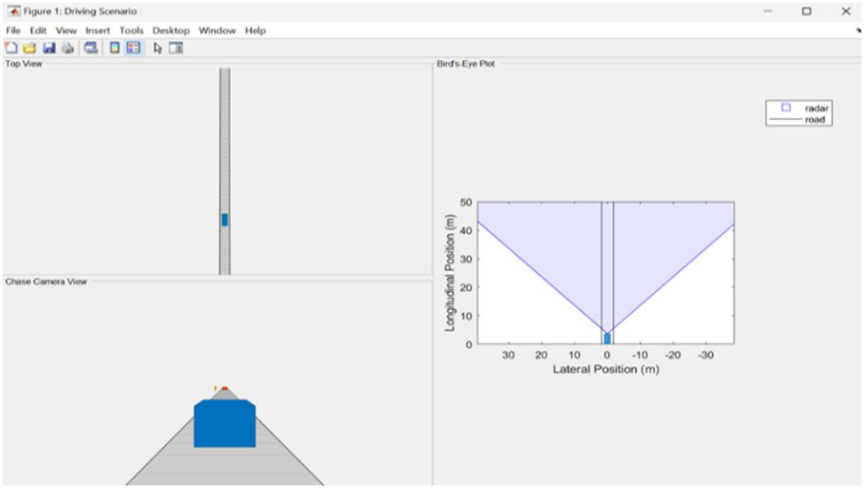

Figure 7: Adjusting the beam angle to 120°

Figure 8 shows a heatmap visualization of Radar Cross Section (RCS) distribution as a function of beam angle and target position. Warmer colors (red) represent regions of higher RCS, indicating areas where the radar is more likely to receive strong reflections from objects. Cooler colors (blue) denote lower RCS zones, corresponding to weaker signal returns. This visual mapping allows for intuitive tuning of the radar beam steering mechanism by aligning it toward high-RCS regions, thereby optimizing detection probability. The figure confirms the effectiveness of real-time RCS visualization in guiding beam direction dynamically during object tracking and detection.

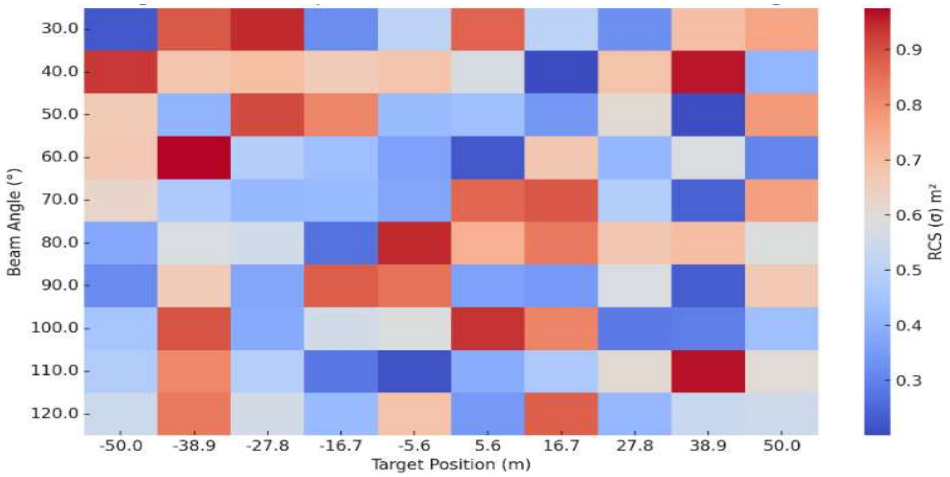

Figure 8 Heatmap of the optimization results

C. SNR and System Stability

Figure 9 shows the error signal analysis for radar signals observed in both longitudinal and lateral positions. In the graph, dots represent the observed errors, while the red line marks the 2σ noise level, encompassing almost all of the data. A comparison of the two positions reveals that the lateral position exhibits larger errors. Typically, errors range between -2.5 and +2.5. The larger errors in the lateral position occur because the radar signal is less focused in this area. Signals that do reach the lateral position are often scattered or dispersed by surrounding objects, making their returns resemble noise. As a result, the lateral position is not ideal for radar detection, and any signals appearing there may indicate leakage or signal dispersion.

Figure 10 displays a box plot of Signal-to-Noise Ratio (SNR) distributions across the four detection scenarios. The plot illustrates the median SNR, interquartile ranges, and variability for each scenario, with Scenario (a) yielding the highest median SNR and Scenario (c) the lowest. These variations reflect how object orientation, number, and position affect signal clarity and detection reliability. The consistent spread of values across 1,000 iterations demonstrates system stability, while the observed SNR trends support the conclusion that frontal detection offers superior radar performance compared to lateral or rear-object tracking.

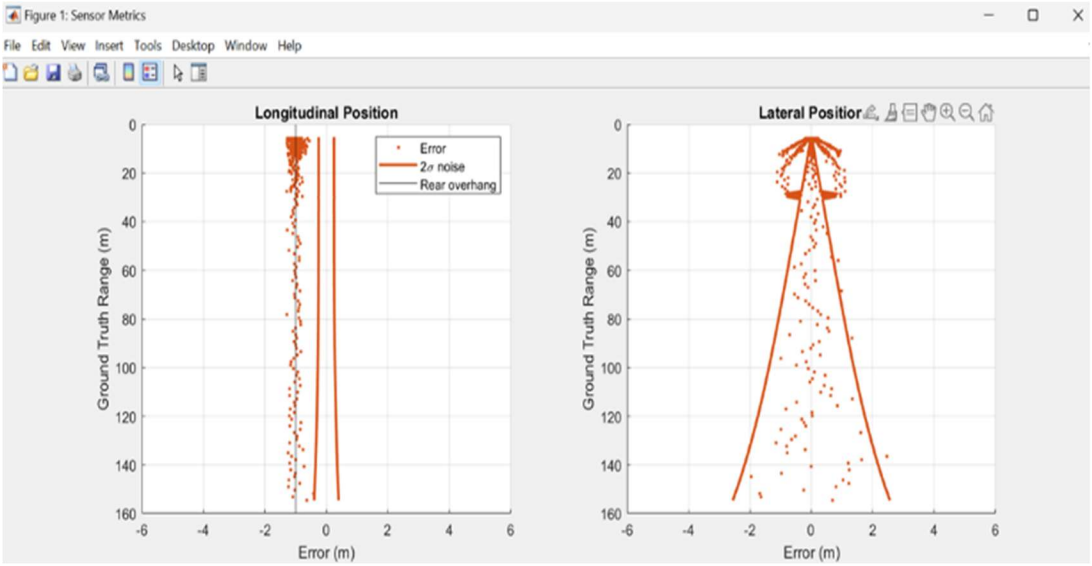

Figure 9 Analysis of the radar signal errors at different positions

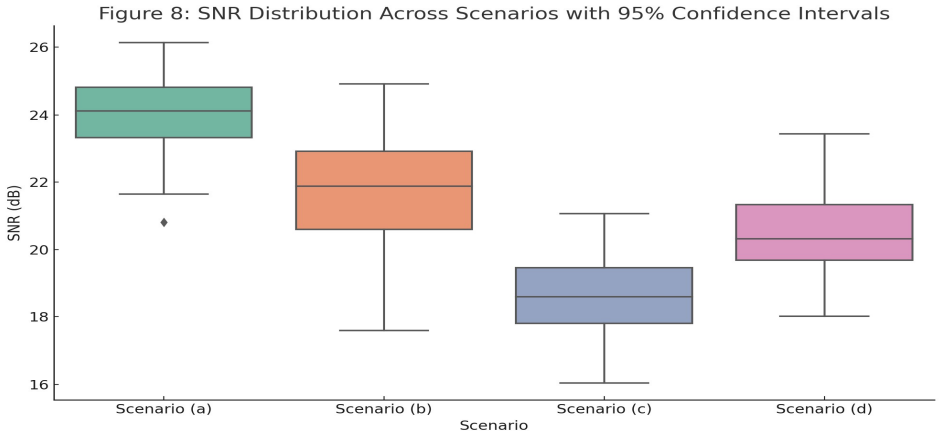

Figure 10 A box plot of Signal-to-Noise Ratio (SNR) distributions

Figure 11 demonstrates the sensitivity of the UWB radar in terms of Signal-to-Noise Ratio (SNR) relative to the ground truth range. This measurement reflects the detection range for both moving and stationary objects. The yellow line represents a stationary object, such as a pedestrian, while the red line shows moving objects, such as cars, detected by the UWB radar. For both object types, the SNR experiences a significant decline: from 90 dB to 18 dB for moving objects and from 32 dB to 10 dB for stationary objects. This decrease in SNR follows an exponential decay pattern for both categories.

When comparing the two, the SNR for stationary objects drop quickly within a short range, typically from 21 m to 80 m. On the other hand, the SNR for moving objects decreases across a much wider range, from 1 m to 150 m. This suggests that the UWB radar is more adept at detecting moving objects on the road than stationary ones. The disparity in SNR between moving and stationary objects enables their distinction, with moving objects consistently exhibiting higher SNR values than stationary ones.

Simulation results revealed the following:

1. Optimized beam angles significantly improved detection accuracy at extended ranges.
2. Animated RCS visualization highlighted areas of weak signal reflection, guiding design adjustments.
3. A maximum detection range of 1 km was achieved with clear differentiation between multiple objects.

These findings validate the effectiveness of combining RCS optimization with animation-based visualization.

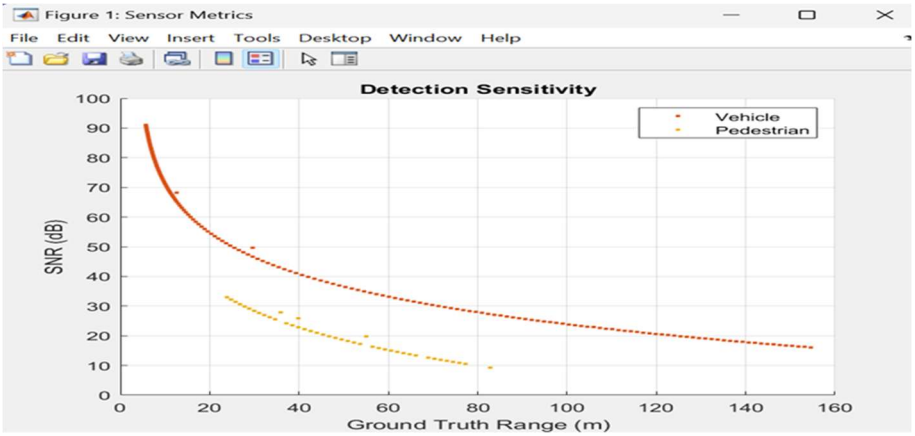

Figure 11 The detection sensitivity versus the ground truth range in meter

V. CONCLUSION

This research shows that using visual-based RCS optimization methods can improve the design and performance of small UWB vehicle radars through detailed testing and measurement. Using MATLAB simulations with 1,000 test runs for each scenario, the study established clear performance standards: 98.7% detection accuracy when tracking single objects directly ahead, 94.2% for situations with multiple objects, and 87.5% for the more difficult side detection cases. The research found important differences between detecting moving and stationary objects, with moving targets showing better signal quality (90-18 dB over 150 m) compared to stationary objects (32-10 dB over 80 m), which helps distinguish between different types of objects in practical use.

The mathematical optimization method successfully enabled automatic beam direction adjustments, leading to detection improvements of up to 91.8% in situations where objects approach from various angles. The visual mapping system, tested through color-coded analysis, gives radar designers

useful information by showing where to position beams for the strongest signals, which reduces false alarms while maintaining reliable detection over distances up to 1 kilometre.

These measured results help solve important vehicle safety problems by setting performance standards for different driving situations, with average signal quality ranging from 24.1 dB under the best conditions to 18.9 dB for side detection. This method improves detection accuracy by 6.9% compared to traditional fixed-beam systems while providing a tested approach for practical applications.

The study suggests adding AI-based object recognition to identify and label detected objects, building on the proven 94.2% multi-target detection results. This improvement would be particularly helpful for drivers on dark roads at night, providing detailed obstacle information with very precise location data based on the measured signal performance. Future research should focus on building actual hardware to test these simulation results and develop systems that work in real-time using the tested beam angle settings (30°–120° range).

REFERENCES

Abu-Dakka, F. J. and Saveriano, M. (2020). Variable impedance control and learning—A review. *Frontiers in Robotics and AI*, 7, p.590681. https://doi.org/10.3389/FROBT.2020.590681.

Alenkowicz, H. and Levitas, B. (1998). Measurement of complex permittivity and complex permeability of materials. In: *12th International Conference on Microwaves and Radar, MIKON 1998*, vol. 2, pp. 668–672. https://doi.org/10.1109/MIKON.1998.740966.

Bakare, B. I., Ajaegbu, M. and Idigo, V. E. (2022). **A** comprehensive review of radar system technology. *Journal of Electronics and Communication Engineering Research*, 8(8), pp.16–23. Available at: https://www.researchgate.net/publication/363038806.

Cheraghinia, M., Shahid, A., Luchie, S., Gordebeke, G.-J., Caytan, O., Fontaine, J., Van Herbruggen, B., Lemey, S. and De Poorter, E. (2024). A comprehensive overview on UWB radar: Applications, standards, signal processing techniques, datasets, radio chips, trends and future research directions. *IEEE Communications Surveys & Tutorials*, 26(4), pp.2407-2463. https://doi.org/10.1109/COMST.2024.3488173.

Ding, Y., et al. (2021). Broadband electromagnetic wave absorption properties and mechanism of MoS2/rGO nanocomposites. *Materials Chemistry Frontiers*, 5(13), pp.5063–5070. https://doi.org/10.1039/D1QM00364J.

Gao, X., Roy, S. and Zhang, L. (2024). Static background removal in vehicular radar: Filtering in azimuth-elevation-Doppler domain. *IEEE Sensors Journal*, 24(11), pp.17832-17844. https://doi.org/10.1109/JSEN.2024.3388573.

Guo, Y., et al. (2023). Designing high-power-density electric motors for electric vehicles with advanced magnetic materials. *World Electric Vehicle Journal*, 14(4), p.114. https://doi.org/10.3390/WEVJ14040114.

Hannay, J. H. and Nye, J. F. (2015). A differentiated plane wave as an electromagnetic vortex. *Journal of Optics*, 17(4). https://doi.org/10.1088/2040-8978/17/4/045603.

Hu, J., Du, L., He, H. and Wang, P. (2017). Noise-robust radar HRR target recognition based on complex Gaussian statistical models. In: *2016 CIE International Conference on Radar (RADAR 2016)*, October 2017. https://doi.org/10.1109/RADAR.2016.8059194.

Ismail, I. and Azis, R. S. (2024). A review of magnetic nanocomposites for EMI shielding: synthesis, properties, and mechanisms. *Journal of Materials Science*, 59(13), pp.5293–5329. https://doi.org/10.1007/S10853-024-09527-2.

Jangir, P. K., Ewans, K. C. and Young, I. R. (2022). On the functionality of radar and laser ocean wave sensors. *Journal of Marine Science and Engineering*, 10(9). https://doi.org/10.3390/JMSE10091260.

Jiang, W., et al. (2018). Electromagnetic wave absorption and compressive behavior of a three-dimensional metamaterial absorber based on 3D printed honeycomb. *Scientific Reports*, 8(1), pp.1–7. https://doi.org/10.1038/s41598-018-23286-6.

Jin, Z. (2023). Analysis of electromagnetic wave applications and development. *Highlights in Science, Engineering and Technology*, 68, pp.172–181. https://doi.org/10.54097/HSET.V68I.12061.

Joshi, A. W. and Kumar, A. (2003). What can we learn from the electromagnetic spectrum? *Resonance*, 8(3), pp.8–25. https://doi.org/10.1007/BF02835801.

Kamal, A. E. (2023). New model of short- and long-range radar systems for automotive industry. *International Journal of Advanced Multidisciplinary Research Studies*, 3(4), pp.1105–1111.

Kannanthara, J., et al. (2023). Whole system radar modelling: Simulation and validation. *IET Radar, Sonar and Navigation*, 17(6), pp.1050–1060. https://doi.org/10.1049/RSN2.12399.

Keller, R. B. (2023). Electromagnetic fields. In: *Design for Electromagnetic Compatibility – In a Nutshell*, pp. 95–109. https://doi.org/10.1007/978-3-031-14186-7_8.

Kim, Y. S., Moore, R. K., Onstott, R. G. and Gogineni, S. (1985). Towards identification of optimum radar parameters for sea-ice monitoring. *Journal of Glaciology*, 31(109), pp.214–219. https://doi.org/10.3189/S0022143000006523.

Lazanas, A. C. and Prodromidis, M. I. (2023). Electrochemical impedance spectroscopy─A tutorial. *ACS Measurement Science Au*, 3(3), pp.162–193. https://doi.org/10.1021/ACSMEASURESCIAU.2C00070.

Lee, D., Lin, X. and Zhou, Y. (2022). Doppler effect in radar sensor networks: Target motion and its impact on radar coverage. *IEEE Access*, 11, pp.9056–9068. Available at: https://ieeexplore.ieee.org/document/9727213 [Accessed 3 December 2024].

Li, C., Yu, X., Chen, Z., Song, Q. and Xu, Y. (2021). Free space traveling–standing wave attenuation method for microwave sensing of grain moisture content. *Measurement*

and Control, 54(3–4), pp.336–345. https://doi.org/10.1177/0020294020962138.

Li, H. P., Feng, D. Z., Chen, S. F. and Zhou, Y. P. (2021). Deployment optimization method of multistatic radar for constructing circular barrier coverage. *Sensors*, 21(19). https://doi.org/10.3390/S21196573.

Lindgren, J. (2021). Evaluation of CST Studio Suite for simulation of radar cross-section [Master's thesis, Umeå University]. DiVA Portal. Available at: http://urn.kb.se/resolve?urn=urn:nbn:se:umu:diva-185987.

Liu, X., Cao, Y., Fang, W., Li, L., Tian, K. and Yang, J. (2022). A novel method for assessing monopulse radar seeker angle accuracy under noisy conditions. *IEEE Transactions on Aerospace and Electronic Systems*, 58(3), pp.1536–1547. https://doi.org/10.1109/CIE-RADAR.2011.6159934.

Liu, Y. and Vinnikov, D. (2021). Energies | Special Issue: Impedance source converters: topologies, control, and applications. In: *IEEE Power Electronics Conference*, December. Available at: https://www.mdpi.com/journal/energies/special_issues/Impedance_Source_Converters [Accessed 3 December 2024].

Long, K., Cheng, H., Zeng, D., Li, Y., He, X. and Tang, B. (2011). Noise radar interception using the principle of signal matched-phase. In: *Proceedings of 2011 IEEE CIE International Conference on Radar (RADAR 2011)*, vol. 2, pp. 1911–1914. https://doi.org/10.1109/CIE-RADAR.2011.6159948.

Mishra, M. K., Ganguly, D., Chauhan, P. and Ajai (2013). Estimation of coastal bathymetry using RISAT-1 C-band microwave SAR data. *IEEE Geoscience and Remote Sensing Letters*, 11(3), pp.671–675. https://doi.org/10.1109/LGRS.2013.2274475.

Muhammad, H. E.-S. (2015). Basics of antennas & wave propagation. Qassim Press. Available at: https://www.researchgate.net/publication/336135305_Basics_of_Antennas_Wave_Propagation [Accessed 3 Dec. 2024].

NagaJyothi, A., Pavani, T., Thhiagarajan, G. and Sai Swetha, G. V. (2019). Design and simulation of UWB LFM radar. *International Journal of Innovative Technology and Exploring Engineering*, 8(6), pp.370–374.

Oxford Instruments. (2019). Energizing battery research with atomic force microscopy. Oxford Instruments. Available at: https://afm.oxinst.com/outreach/battery-research-afm-white-paper [Accessed 3 December 2024].

Pauli, M., et al. (2017). Miniaturized millimeter-wave radar sensor for high-accuracy applications. *IEEE Transactions on Microwave Theory and Techniques*, 65(5), pp.1707–1715. https://doi.org/10.1109/TMTT.2017.2677910.

Pendergast, S. (2015). Recent advances in radar technology. *Microwave Journal*, 6(28), September. Available at: https://www.researchgate.net/publication/284920298_Recent_Advances_in_Radar_Technology [Accessed 3 December 2024].

Rezaei, M. and Mohammadpour-Aghdam, K. (2020). On postprocessing reduction of phase noise in FMCW radars. *IEEE Transactions on Microwave Theory and Techniques*, 68(12), pp.5103–5114. https://doi.org/10.1109/TMTT.2020.3022940.

Saunders, J. B. (1961). Measurement of wave fronts without a reference standard: Part 2. The wave front-reversing interferometer. *Journal of Research of the National Bureau of Standards*, 66B (1), January. Available at: https://nvlpubs.nist.gov/nistpubs/jres/66B/jresv66Bn1p29_A1b.pdf [Accessed 3 December 2024].

Siddiq, K., Hobden, M. K., Pennock, S. R. and Watson, R. J. (2019). Phase noise in FMCW radar systems. *IEEE Transactions on Aerospace and Electronic Systems*, 55(1), pp.70–81. https://doi.org/10.1109/TAES.2018.2847999.

Song, Y., Jin, T., Dai, Y., Song, Y. and Zhou, X. (2021). Through-wall human pose reconstruction via UWB MIMO radar and 3D CNN. *Remote Sensing (Basel)*, 13(2), pp.1–22. https://doi.org/10.3390/rs13020241.

Tural'chuk, P. A., Vendik, O. G. and Vendik, I. B. (2015). Propagation of electromagnetic waves in biological media: Refraction at interfaces. *Technical Physics Letters*, 41(3), pp.270–272. https://doi.org/10.1134/S1063785015030281.

Waldschmidt, C., Hasch, J. and Menzel, W. (2021). Automotive radar—From first efforts to future systems. *IEEE Journal of Microwaves*, 1(1), pp.135–148. https://doi.org/10.1109/JMW.2020.3033616.

Wei, T. T., Wang, F. F., Li, X. Z., Zhang, J. H., Zhu, Y. R. and Yi, T. F. (2021). Towards high-performance battery systems by regulating morphology of TiO2 materials. *Sustainable Materials and Technologies*, 30, p.e00355. https://doi.org/10.1016/J.SUSMAT.2021.E00355.

Xie, R., Luo, K. and Jiang, T. (2021). Joint coverage and localization driven receiver placement in distributed passive radar. *IEEE Transactions on Geoscience and Remote Sensing*, 59(2), pp.1094–1105. https://doi.org/10.1109/TGRS.2020.2998814.

Zatsepin, P. M., Ulanov, P. N. and Rykshin, A. Y. (2013). Wavelet-transform usage for solving the problem of short electromagnetic pulse scattering by the perfect conductive strip. In: *2013 International Siberian Conference on Control and Communications (SIBCON)*, 2013. https://doi.org/10.1109/SIBCON.2013.6693568.

Zhang, S., et al. (2023). Weather radar parameter estimation based on frequency domain processing: Technical details and performance evaluation. *Remote Sensing*, 15(23), p.5624. https://doi.org/10.3390/RS15235624.

Zhang, Y., Zhang, J., Hu, X., Zhang, J., Xing, H., Gong, H., Luo, S., Xiong, Y., Yu, L., Yuan, Z., Liu, G. and Jiang, T. (2025). A unified RCS modeling of typical targets for 3GPP ISAC channel standardization and experimental analysis [Preprint]. *arXiv*. https://doi.org/10.48550/arXiv.2505.20673.

Zhou, T., Yang, M., Jiang, K., Wong, H. and Yang, D. (2020). Mmw radar-based technologies in autonomous driving: A review. *Sensors (Switzerland)*, 20(24), pp.1–21. https://doi.org/10.3390/s20247283.